An approach to retrieve BRDF from satellite and airborne measurements of surface-reflected radiance based on decoupling of atmospheric radiative transfer and surface reflection

Alexander Radkevich
Science Systems and Applications, Inc., 1 Enterprise Parkway, Hampton, VA, USA 23666

ABSTRACT

Bi-directional Reflection Distribution Function (BRDF) defines anisotropy of the surface reflection. It is required to specify the boundary condition for radiative transfer (RT) modeling. Measurements of reflected radiance by satellite- and air-borne sensors provide information about anisotropy of surface reflection. Atmospheric correction needs to be performed to derive BRDF from the reflected radiance. Common approach for BRDF retrievals consists of the use of kernel-based BRDF and RT modeling that needs to be done anew at every step of the iterative process. The kernels' weights are obtained by minimization of the difference between measured and modeled radiance. This study develops a new method of retrieving kernel-based BRDF that requires RT calculations to be done only once.

The method employs the exact analytical expression of radiance at any atmospheric level through the solutions of two auxiliary atmosphere-only RT problems and the surface-reflected radiance at the surface level. The latter is related to BRDF and solutions of the auxiliary RT problems by a Fredholm integral equation of the second kind. The approach requires to perform RT calculations one time before the iterations. It can use observations taken at different atmospheric conditions assuming that surface conditions remain unchanged during the time span of observations. The algorithm accurately catches zero weights of the kernels that may be a concern if the number of kernels is greater than 3 in current mainstream approaches. The study presents numerical tests of the BRDF retrieval algorithm for various surface and atmospheric conditions.

Keywords: earth surface, BRDF retrieval, atmospheric correction, atmosphere-surface decoupling

1. INTRODUCTION

Radiation reflected from the Earth's surface presents a valuable source of information about surface properties that can be formalized in the bi-directional reflection distribution function (BRDF). BRDF is required to specify the boundary condition for radiative transfer (RT) modeling used in aerosol retrievals [1], cloud retrievals [2], and other applications, see e.g. [3].

MODIS BRDF retrieval algorithm [4] was the first operational BRDF retrieval algorithm. Wanner et al. [5] provided theoretical basis of the retrieval process. That study underscores importance of the surface-atmosphere coupling and the need of decoupling. The approach of the algorithm is to perform atmospheric correction to obtain reflectance at the surface level then finding the least square match with kernel-based BRDF model. Formulation of the atmospheric correction in that approach was suggested by Vermote et al. [6]. TOA reflectance is presented there as a sum of the path radiance and surface-reflected radiance. The latter is expressed in the fashion of the case of Lambertian surface reflection with an attempt to replace albedo in the exact formula by directional reflectance and its mean values, see Eq. (1) of [5]. That expression was postulated but has never been derived directly from the radiative transfer equation (RTE) and supplementing boundary conditions. Therefore, its accuracy can only be evaluated numerically in particular cases.

Another BRDF retrieval algorithm is a part of multi-angle implementation of atmospheric correction (MAIAC) [7, 8, 9]. Unlike MODIS BRDF algorithm, MAIAC matches modeled and observed radiance at the level of observation rather than at the surface using an iterative scheme. That algorithm uses decoupling presenting total surface reflectance as a series by the number of reflections from the surface [10] (not to be confused with the number of scatterings in atmospheric RT). MAIAC then uses an approximate expression of the reflected radiance at the surface, see Eq. (2) of [7]. The approximation originates from the necessity to summate the series by the number of reflections. The accuracy of that approximation was found high [10].

In this study yet another algorithm will be developed. It is based on exact analytical decoupling of surface reflection and atmospheric RT [11]. The key feature of the approach is an integral equation governing surface-reflected radiance at the surface level. It was showed that solution of the equation is the informal sum of the series by the number of reflections presented in [10]. Thus, it removes the necessity to use approximation of the sum used in MAIAC. At the same time, it removes the necessity to use multiple assumptions of atmospheric correction procedure used in MODIS BRDF algorithm. The algorithm can be seen as an extension of a recently developed algorithm for BRDF retrieval from ground measurements of reflected radiance [12].

The use of kernel-based model became a standard approach in BRDF retrieval algorithms, see, e.g. [13, 14, 15]. Most of the models are comprised with three kernels though Liu and co-authors presented a five-kernel model [16]. An overview of the modern state of the field is given in Roujean [17]. In particular, that study argued that "the BRDF model matrix is ill-conditioned if the number of kernels would be too much in exceed over three because of their similarity, which leads to linear dependence of model kernels. Therefore, further progress in BRDF modeling and inversion is related to these model extensions and implementation of advanced inversion techniques." One such inversion technique will be developed in this project. Study [17] also states "the kernels could be of any kind of complexity, provided they properly and correctly mimic the observed information", so that selection of kernels for the retrieval model is an important problem that should be addressed based on physical features of the surface. However, this problem is out of scope of this study and will not be considered here. The purpose of the development here is to present an algorithm for obtaining kernel weights in a situation when the choice of the kernels is clear.

2. THEORETICAL BASIS OF THE ALGORITHM

2.1 Boundary value problems to the radiative transfer equation

Let us consider an atmosphere underlain with anisotropic reflective surface at its bottom and illuminated with broad light flux coming from a single direction. Then radiance L within the atmosphere and its boundaries is defined by the radiative transfer equation

$$\mu\frac{\partial L_T}{\partial\tau}+L_T(\tau,\mu,\phi\,|\,\tau_t,\mu_0)=\Lambda(\tau)\int_0^{2\pi}d\phi'\int_{-1}^{1}d\mu'\chi(\tau,\mu',\mu,\phi'-\phi)L_T(\tau,\mu',\phi'\,|\,\tau_t,\mu_0) \tag{1}$$

supplemented with boundary conditions

$$L_T(\tau=0,\mu>0,\phi\,|\,\tau_t,\mu_0)=I_0\delta(\mu-\mu_0)\delta(\phi),\quad \mu_0>0 \tag{2}$$

$$L_T(\tau=\tau_t,\mu<0,\phi\,|\,\tau_t,\mu_0)=\int_0^{2\pi}d\phi'\int_0^{1}d\mu'\rho(\mu',|\mu|,\phi'-\phi)\mu' L_T(\tau=\tau_t,\mu',\phi'\,|\,\tau_t,\mu_0) \tag{3}$$

Subscript $_T$ refers to the total (direct and diffuse) radiance. It will be necessary to distinguish solutions of the boundary value problems (BVPs) under different atmospheric conditions and different directions of illumination. For this reason total optical thickness of the atmosphere, τ_t, and cosine of the solar zenith angle (SZA), μ_0, are added as parameter arguments of radiance separated by the vertical bar from the other arguments. Later, a subscript will be added to these variables to specify different observations. Also in Eqs. (1) – (3): τ is optical depth, μ - cosine of viewing zenith angle (VZA), ϕ - relative azimuth angle between directions from the sun and to the observer, $\Lambda(\tau)$ - single scattering albedo, $\chi(\tau,\mu',\mu,\phi'-\phi)$ - scattering phase function, $\rho(\mu',|\mu|,\phi'-\phi)$ - BRDF. The top surface illuminated with monodirectional light with irradiance of $I_0\mu_0$.

For further development we will need to consider two auxiliary RT problems: the same atmosphere without reflection at the bottom surface and flipped over atmosphere without reflection at the bottom surface. We will denote the solutions of these problems as *I* and *J*, respectively. Mathematical formulation of these two problems is given below.

$$\mu\frac{\partial I_T}{\partial\tau}+I_T(\tau,\mu,\phi\,|\,\tau_t,\mu_0)=\Lambda(\tau)\int_0^{2\pi}d\phi'\int_{-1}^{1}d\mu'\chi(\tau,\mu',\mu,\phi'-\phi)I_T(\tau,\mu',\phi'\,|\,\tau_t,\mu_0) \tag{4}$$

$$I_T(\tau=0,\mu>0,\phi\,|\,\tau_t,\mu_0)=I_0\delta(\mu-\mu_0)\delta(\phi),\quad \mu_0>0 \tag{5}$$

$$I_T(\tau=\tau_t,\mu<0,\phi\,|\,\mu_0)=0 \tag{6}$$

$$\mu\frac{\partial J_T}{\partial\tau}+J_T(\tau,\mu,\phi\,|\,\tau_t,\mu_0)=\Lambda(\tau_t-\tau)\int_0^{2\pi}d\phi'\int_{-1}^{1}d\mu'\chi(\tau_t-\tau,\mu',\mu,\phi'-\phi)J_T(\tau,\mu',\phi'\,|\,\tau_t,\mu_0) \tag{7}$$

$$J_T(\tau=0,\mu>0,\phi\,|\,\tau_t,\mu_0)=\delta(\mu-\mu_0)\delta(\phi),\quad \mu_0>0 \tag{8}$$

$$J_T(\tau=\tau_t,\mu<0,\phi\,|\,\tau_t,\mu_0)=0 \tag{9}$$

Please note that the top surface boundary condition in the last problem differs from those in the first two by the factor of I_0. Separating direct and diffuse light in all three problems as

$$L_T(\tau,\mu,\phi\,|\,\tau_t,\mu_0)=I_0\delta(\mu-\mu_0)\delta(\phi)\exp(-\tau/\mu_0)+L(\tau,\mu,\phi\,|\,\tau_t,\mu_0) \tag{10}$$

$$I_T(\tau,\mu,\phi\,|\,\tau_t,\mu_0)=I_0\delta(\mu-\mu_0)\delta(\phi)\exp(-\tau/\mu_0)+I(\tau,\mu,\phi\,|\,\tau_t,\mu_0) \tag{11}$$

$$J_T(\tau,\mu,\phi\,|\,\tau_t,\mu_0)=\delta(\mu-\mu_0)\delta(\phi)\exp(-\tau/\mu_0)+J(\tau,\mu,\phi\,|\,\tau_t,\mu_0) \tag{12}$$

2.2 Decoupling of decoupling of atmospheric radiative transfer and surface reflection

Diffuse radiance $L(\tau,\mu,\phi\,|\,\tau_t,\mu_0)$ at any level can be expressed through its value at the reflecting surface $L(\tau=\tau_t,\mu<0,\phi\,|\,\tau_t,\mu_0)$ and auxiliary radiances $I(\tau,\mu,\phi\,|\,\tau_t,\mu_0)$ and $J(\tau,\mu,\phi\,|\,\tau_t,\mu_0)$ [11]:

$$\begin{aligned}L(\tau,\mu,\phi\,|\,\tau_t,\mu_0)&=I(\tau,\mu,\phi\,|\,\tau_t,\mu_0)+\eta(-\mu)\exp[(\tau_t-\tau)/\mu]L(\tau_t,\mu,\phi\,|\,\tau_t,\mu_0)+\\&+\int_0^{2\pi}d\phi''\int_0^{1}d\mu''L(\tau_t,-\mu'',\phi''\,|\,\tau_t,\mu_0)J(\tau_t-\tau,-\mu,\phi-\phi''\,|\,\tau_t,\mu'')\end{aligned} \tag{13}$$

Reflected radiance at the ground level $L(\tau=\tau_t,\mu<0,\phi\,|\,\tau_t,\mu_0)$ is defined with the following integral equation:

$$L(\tau_t,\mu<0,\phi\,|\,\tau_t,\mu_0)=S(\mu<0,\phi\,|\,\tau_t,\mu_0)+\int_0^{2\pi}d\phi''\int_0^{1}d\mu''K(\mu,\mu'',\phi-\phi''\,|\,\tau_t)L(\tau_t,-\mu'',\phi''\,|\,\tau_t,\mu_0) \tag{14}$$

The source function *S* and kernel *K* of this equation depend on radiances *I* and *J*, and BRDF:

$$S(\mu<0,\phi\,|\,\tau_t,\mu_0)=I_0\mu_0\exp(-\tau_t/\mu_0)\rho(\mu_0,|\mu|,\phi)+\int_0^{2\pi}d\phi'\int_0^{1}d\mu'I(\tau_t,\mu',\phi'\,|\,\tau_t,\mu_0)\mu'\rho(\mu',|\mu|,\phi'-\phi) \tag{15}$$

$$K(\mu,\mu'',\phi-\phi''\,|\,\tau_t)=\int_0^{2\pi}d\tilde{\phi}\int_0^{1}d\mu'\rho(\mu',|\mu|,\tilde{\phi}-(\phi-\phi''))\mu'J(\tau=0,-\mu',\tilde{\phi}\,|\,\tau_t,\mu'') \tag{16}$$

Eqs. (13) – (14) along with definitions (15) and (16) express solution to BVP (1) – (3) through solutions of BVPs (4) – (6), *I*, and (7) – (9), *J*, and BRDF ρ.

Physical sense of the last two terms in the right-hand side of Eq. (13) is clear. The first term gives contribution of the light that did not interact with the surface, the 2nd term describes radiation that reaches the detector directly from the surface without atmospheric scattering while the 3rd term is responsible for propagation of the surface reflected radiance with atmospheric interactions as $J(\tau_t-\tau,-\mu,\phi-\phi''\,|\,\tau_t,\mu'')$ gives radiance in direction $(-\mu,\phi)$ caused by unit source illumination flipped-over atmosphere in direction (μ'',ϕ''). It is useful to re-arrange that integral term in Eq. (13) using that the integrands are even and periodic functions of their azimuth variables. Then, it takes the form that will be used in further development:

$$L(\tau,\mu,\phi\,|\,\tau_t,\mu_0) = I(\tau,\mu,\phi\,|\,\tau_t,\mu_0) + \eta(-\mu)\exp[(\tau_t-\tau)/\mu]L(\tau_t,\mu,\phi\,|\,\tau_t,\mu_0) + \int_0^{2\pi} d\phi'' \int_0^1 d\mu'' L(\tau_t,-\mu'',\phi-\phi''\,|\,\tau_t,\mu_0) J(\tau_t-\tau,-\mu,\phi''\,|\,\tau_t,\mu'') \tag{17}$$

Eqs. (17) and (14) allow one to express the solution of the main BVP given by Eqs. (1) - (3) through solutions of the auxiliary BVPs defined with Eqs. (4) – (9). Therefore, this approach allows to solve atmosphere-only problems first and then find solutions to the coupled problem with different BRDFs without solving main BVP directly if the only change in it is BRDF.

2.3 Algorithm assumptions

The approach presented here assumes that BRDF can be expressed as an a priori unknown linear combination of N known kernels:

$$\rho(\mu_1,\mu_2,\phi_1-\phi_2) = \sum_l^N \alpha_l \rho_l(\mu_1,\mu_2,\phi_1-\phi_2)\,, \tag{18}$$

where kernels $\rho(\mu_1,\mu_2,\phi_1-\phi_2)$ are considered symmetric functions with respect to substitution $\mu_1 \Leftrightarrow \mu_2$ and even and periodic functions of its third argument with period of 2π.

Development from section 2.2 was used to retrieve BRDF from the ground observations provided that atmospheric conditions are known [**Error! Reference source not found.**]. The goal of this study is to generalize of that approach for the case of radiance measurements performed at different moments of time with different atmospheric and illumination conditions during a period of time when it is reasonable to assume surface conditions remain unchanged. We will also assume that measurements can be done at different altitudes like it happens during aerial observation campaigns. We will assume that:

the number of measurements is greater than the number of BRDF kernels;

atmospheric conditions are known for all observations, so that auxiliary BVPs can be solved for all of them;

surface is uniform, no 3D effects will be taken into consideration.

Under these assumptions we will denote measured radiance as $L_s = L(\tau_s,\mu_s,\phi_s\,|\,\tau_{t,s},\mu_{0,s})$, where subscript $_s$ denotes the number of a measurement, s = 1, …, M; τ_s is the optical depth at which the measurement was performed, $\tau_{t,s}$ is total optical thickness of the atmosphere, $(\mu_s<0,\phi_s)$ defines the direction of the observation, $\mu_{0,s}$ is cosine of the SZA at the moment of observation.

2.4 BRDF retrieval algorithm

Variations of BRDF change estimations of the observed radiance but they do not change the path radiance (first term on right-hand side of Eq. (17)). It is convenient to subtract computed path radiance from the observed radiance L and introduce surface-reflected radiance ΔL as

$$\Delta L(\tau,\mu,\phi\,|\,\tau_t,\mu_0) \equiv L(\tau,\mu,\phi\,|\,\tau_t,\mu_0) - I(\tau,\mu,\phi\,|\,\tau_t,\mu_0) \tag{19}$$

Then for the position and geometry of observation given by τ_s, $\mu_s<0$, ϕ_s, $\mu_{0,s}$ and optical thickness $\tau_{t,s}$ we obtain

$$\Delta L(\tau_s,\mu_s<0,\phi_s\,|\,\tau_{t,s},\mu_{0,s}) = \exp[(\tau_{t,s}-\tau_s)/\mu_s]L(\tau_{t,s},\mu_s<0,\phi_s\,|\,\tau_{t,s},\mu_{0,s}) + \int_0^{2\pi} d\phi'' \int_0^1 d\mu'' L(\tau_{t,s},-\mu'',\phi_s-\phi''\,|\,\tau_{t,s},\mu_{0,s}) J(\tau_{t,s}-\tau_s,-\mu_s,\phi''\,|\,\tau_{t,s},\mu'') \tag{20}$$

Right-hand side of Eq. (20) is a linear operator of propagation of the reflected radiance from the surface to the level of observation. It will be showed below that the surface-reflected radiance at the surface level is a linear combination of

components associated with the kernels of BRDF ρ_l. Therefore, surface reflected radiance at the level of observation is also a linear combination of components associated with kernels ρ_l.

The basis of the algorithm is minimization of a merit function

$$\varepsilon^2 = \sum_{s=1}^{M} \left(\Delta L_s(\tau_s, \mu_s < 0, \phi_s \mid \tau_{t,s}, \mu_{0,s}) - \Delta L^{(n)}(\tau_s, \mu_s < 0, \phi_s \mid \tau_{t,s}, \mu_{0,s}) \right)^2 \tag{21}$$

where $\Delta L_s(\tau_s, \mu_s < 0, \phi_s \mid \tau_{t,s}, \mu_{0,s})$ is surface-reflected radiance for observation "*s*" computed with definition (19) and $\Delta L^{(n)}(\tau_s, \mu_s < 0, \phi_s \mid \tau_{t,s}, \mu_{0,s})$ is its approximation at the n^{th} step of the algorithm based on Eqs. (20) and (14), and kernel representation of BRDF (18). It is important to mention that approximation $\Delta L^{(n)}$ linearly depends on the set of the kernel weights $\alpha_l^{(n)}$. Routine to construct this approximation is given below.

Eq. (14) for the surface-reflected radiance at the ground level $L(\tau = \tau_t, \mu < 0, \phi \mid \tau_t, \mu_0)$ was studied in [21]. It was showed that under relatively clear sky condition contribution of the integral term in right-hand side of Eq. (14) is small though it cannot be neglected. In the BRDF retrieval algorithm it will be neglected only at the initial step of the iterative process. Using kernel representation of BRDF (18) we obtain a formal initial guess of the reflected radiance at the surface level for each observation $L(\tau_{t,s}, \mu < 0, \phi \mid \tau_{t,s}, \mu_{0,s})$:

$$L^{(0)}(\tau_{t,s}, \mu < 0, \phi \mid \tau_{t,s}, \mu_{0,s}) = \sum_{l}^{N} \alpha_l^{(0)} S_l(\mu < 0, \phi \mid \tau_{t,s}, \mu_{0,s}) \tag{22}$$

(not to be confused with upwelling surface-reflected radiance at the level of observation $\Delta L^{(0)}(\tau_s, \mu_s < 0, \phi_s \mid \tau_{t,s}, \mu_{0,s})$ from Eq. (21)). Here $S_l(\mu < 0, \phi \mid \tau_{t,s}, \mu_{0,s})$ are components of the source function $S(\mu < 0, \phi \mid \tau_{t,s}, \mu_{0,s})$, see Eq. (15), associated with BRDF kernels ρ_l:

$$\begin{aligned} S_l(\mu < 0, \phi \mid \tau_{t,s}, \mu_{0,s}) &= I_0 \mu_{0,s} \rho_l(\mu_{0,s}, \mid \mu \mid, \phi) \exp(-\tau_{t,s} / \mu_{0,s}) \\ &+ \int_0^{2\pi} d\phi' \int_0^1 d\mu' I(\tau_{t,s}, \mu', \phi' \mid \tau_{t,s}, \mu_{0,s}) \mu' \rho_l(\mu', \mid \mu \mid, \phi' - \phi) \end{aligned} \tag{23}$$

Expression (22) is formal until the values of the kernel weights $\alpha_l^{(0)}$ are not specified. In order to find them we need to express upwelling surface-reflected radiance at the level observation through the weights. We obtain from Eqs, (20) and (22) for measurement "*s*":

$$\Delta L^{(0)}(\tau_s, \mu_s < 0, \phi_s \mid \tau_{t,s}, \mu_{0,s}) = \sum_{l}^{N} \alpha_l^{(0)} \Delta L_l^{(0)}(\tau_s, \mu_s < 0, \phi_s \mid \tau_{t,s}, \mu_{0,s}) \tag{24}$$

where

$$\begin{aligned} \Delta L_l^{(0)}(\tau_s, \mu_s < 0, \phi_s \mid \tau_{t,s}, \mu_{0,s}) &= \exp[(\tau_s - \tau_{t,s}) / \mid \mu_s \mid] S_l(\mu_s < 0, \phi_s \mid \tau_{t,s}, \mu_{0,s}) \\ &+ \int_0^{2\pi} d\phi'' \int_0^1 d\mu'' S_l(-\mu'', \phi_s - \phi'' \mid \tau_{t,s}, \mu_{0,s}) J(\tau_{t,s} - \tau_s, -\mu_s, \phi'' \mid \tau_{t,s}, \mu'') \end{aligned} \tag{25}$$

All functions on the right-hand side of the Eq. (25) are known once the auxiliary BVPs are solved. Now the kernel weights $\alpha_l^{(0)}$ can be found by minimization of the merit function given by Eq. (21). After that Eq. (22) gives values of initial approximation of the surface-reflected radiance at the surface level $L^{(0)}(\tau_{t,s}, \mu < 0, \phi \mid \tau_{t,s}, \mu_{0,s})$. These operations of the initial step can be repeated with taking into account the integral term of Eq. (14) using previous step estimate $L^{(n-1)}(\tau_{t,s}, \mu < 0, \phi \mid \tau_{t,s}, \mu_{0,s})$ to evaluate $L^{(n)}(\tau_{t,s}, \mu < 0, \phi \mid \tau_{t,s}, \mu_{0,s})$.

The stages of the n^{th} step are formalized as follow. First, formal expression of the reflected radiance at the surface level

$$L^{(n)}(\tau_{t,s},\mu<0,\phi\,|\,\tau_{t,s},\mu_{0,s})=\sum_{l}^{N}\alpha_l^{(n)}L_l^{(n)}(\tau_{t,s},\mu<0,\phi\,|\,\tau_{t,s},\mu_{0,s}) \tag{26}$$

with auxiliary functions $L_l^{(n)}$ are defined as

$$\begin{aligned}L_l^{(n)}(\tau_{t,s},\mu<0,\phi\,|\,\tau_{t,s},\mu_{0,s})&=S_l(\mu<0,\phi\,|\,\tau_{t,s},\mu_{0,s})\\&+\int_0^{2\pi}d\phi''\int_0^1 d\mu''K_l(\mu,\mu'',\phi-\phi''\,|\,\tau_{t,s})L^{(n-1)}(\tau_{t,s},-\mu'',\phi''\,|\,\tau_{t,s},\mu_{0,s})\end{aligned} \tag{27}$$

$$K_l(\mu,\mu'',\phi-\phi''\,|\,\tau_t)=\int_0^{2\pi}d\tilde{\phi}\int_0^1 d\mu'\rho_l(\mu',|\mu|,\tilde{\phi}-(\phi-\phi''))\mu' J(\tau=0,-\mu',\tilde{\phi}\,|\,\tau_t,\mu'') \tag{28}$$

This leads to the following expression for the surface-reflected radiance at the level of observation:

$$\Delta L^{(n)}(\tau_s,\mu<0,\phi\,|\,\tau_{t,s},\mu_{0,s})=\sum_{l}^{N}\alpha_l^{(n)}\Delta L_l^{(n)}(\tau_s,\mu<0,\phi\,|\,\tau_{t,s},\mu_{0,s}) \tag{29}$$

where

$$\begin{aligned}\Delta L_l^{(n)}(\tau_s,\mu_s<0,\phi_s\,|\,\tau_{t,s},\mu_{0,s})&=\exp[(\tau_s-\tau_{t,s})/|\mu_s|]L_l^{(n)}(\tau_{t,s},\mu_s<0,\phi_s\,|\,\tau_{t,s},\mu_{0,s})\\&+\int_0^{2\pi}d\phi''\int_0^1 d\mu''L_l^{(n)}(\tau_{t,s},-\mu'',\phi_s-\phi''\,|\,\tau_{t,s},\mu_{0,s})J(\tau_{t,s}-\tau_s,-\mu_s,\phi''\,|\,\tau_{t,s},\mu'')\end{aligned} \tag{30}$$

So, Eqs. (26) and (27) enable n^{th} approximation of the BRDF kernel weights $\{\alpha_l^{(n)}\}$ by minimization of the merit function given by Eq. (21) that takes the form

$$\varepsilon^2=\sum_{s=1}^{M}\left(\Delta L_s(\tau_s,\mu_s<0,\phi_s\,|\,\tau_{t,s},\mu_{0,s})-\sum_{l}^{N}\alpha_l^{(n)}\Delta L_l^{(n)}(\tau_s,\mu_s<0,\phi_s\,|\,\tau_{t,s},\mu_{t,s})\right)^2 \tag{31}$$

3. NUMERICAL IMPLEMENTATION OF THE ALGORITHM

3.1 Quadrature rules

At the beginning of numerical implementation a quadrature rule needs to be selected to perform numerical integration over a hemisphere. While efficient quadratures on a hemisphere can be developed in this study a direct product of two 1D quadrature rules will be employed. Integration over polar angle will be performed by means of Gaussian quadrature scaled to [0, 1] interval so that $\{\mu_i,w_i\}_{i=1}^{p}$ are pairs of nodes and their weights, respectively and $\sum_{i=1}^{p}w_i=1$.

For integration over azimuth we will take into account that functions involved in the equations above are periodic and symmetric functions of the azimuth angle ϕ. Keeping in mind the goal to minimize the number of necessary atmospheric radiative transfer computations, namely the number of argument values at which radiances *I* and *J* need to be computed, we will use the following relationship .

$$g(\phi_s)=\int_0^{2\pi}d\phi' f_1(\phi')\,f_2(\phi'-\phi_s)=\int_0^{\pi}d\phi' f_1(\phi')[\,f_2(\phi'+\phi_s)+\,f_2(\phi'-\phi_s)] \tag{32}$$

For integration over azimuth trapezoid rule will be used on an equidistant grid

$$\begin{aligned}\phi_j&=\pi(j-1)/(m-1)\\\beta_j&=\pi/(m-1)[1-1/2(\delta_{j,1}+\delta_{j,m})]\end{aligned} \tag{33}$$

where $\delta_{q,r}$ is the Kronecker delta and *m* is the total number of nodes.

Let's consider discretization of surface-reflected radiance related to the BRDF kernel ρ_l given by Eq. (30):

$$\begin{aligned}\Delta L_l^{(n)}(\tau_s,\mu_s<0,\phi_s\,|\,\tau_{t,s},\mu_{0,s}) &= \exp[(\tau_s-\tau_{t,s})/|\mu_s|]L_l^{(n)}(\tau_{t,s},\mu_s<0,\phi_s\,|\,\tau_{t,s},\mu_{0,s})\\ &+\sum_j^m\sum_i^p w_i\beta_j\left[L_l^{(n)}(\tau_{t,s},-\mu_i,\phi_s-\phi_j\,|\,\tau_{t,s},\mu_{0,s})+L_l^{(n)}(\tau_{t,s},-\mu_i,\phi_s+\phi_j\,|\,\tau_{t,s},\mu_{0,s})\right]J(\tau_{t,s}-\tau_s,-\mu_s,\phi_j\,|\,\tau_{t,s},\mu_i)\end{aligned} \tag{34}$$

So, pre-computed values $J(\tau_{t,s}-\tau_s,-\mu_s,\phi_j\,|\,\tau_{t,s},\mu_i)$ are needed to evaluate the second term on the right-hand side. That evaluation also requires surface-reflected kernel-related radiances $L_l^{(n)}(\tau_{t,s},\mu_s<0,\phi_s\,|\,\tau_{t,s},\mu_{t,s})$ and $L_l^{(n)}(\tau_{t,s},-\mu_i,\phi_s\pm\phi_j\,|\,\tau_{t,s},\mu_{0,s})$. These values can be obtained from the discretized version of Eq. (27)

$$\begin{aligned}L_l^{(n)}(\tau_{t,s},\mu<0,\phi\,|\,\tau_{t,s},\mu_{0,s}) &= S_l(\mu<0,\phi\,|\,\tau_{t,s},\mu_{0,s})\\ &+\sum_i^p\sum_j^m w_i\beta_j\tilde{K}_l(\mu,\mu_i,\phi,\phi_j\,|\,\tau_{t,s})L^{(n-1)}(\tau_{t,s},-\mu_i,\phi_j\,|\,\tau_{t,s},\mu_{0,s})\end{aligned} \tag{35}$$

where source functions S_l are evaluated with discretized version of Eq. (23)

$$\begin{aligned}S_l(\mu<0,\phi\,|\,\tau_{t,s},\mu_{0,s}) &= I_0\mu_{0,s}\exp(-\tau_{t,s}/\mu_{0,s})\rho_l(\mu_{0,s},|\mu|,\phi)\\ &+\sum_i^p\sum_j^m w_i\beta_j I(\tau_{t,s},\mu_i,\phi_j\,|\,\tau_{t,s},\mu_{0,s})\mu_i\tilde{\rho}_l(\mu_i,|\mu|,\phi_j,\phi)\end{aligned} \tag{36}$$

$$\tilde{\rho}(\mu_1,\mu_2,\phi_1,\phi_2)=\rho(\mu_1,\mu_2,\phi_1-\phi_2)+\rho(\mu_1,\mu_2,\phi_1+\phi_2) \tag{37}$$

$$\tilde{K}_l(\mu,\mu_i,\phi,\phi_j\,|\,\tau_{t,s})=K_l(\mu,\mu_i,\phi-\phi_j\,|\,\tau_{t,s})+K_l(\mu,\mu_i,\phi+\phi_j\,|\,\tau_{t,s}) \tag{38}$$

Kernel-related components of the kernel *K* are evaluated with the discretized version of Eq. (28)

$$K_l(\mu,\mu'',\tilde{\phi}\,|\,\tau_{t,s})=\sum_{q=1}^p\sum_{r=1}^m w_q\beta_r\tilde{\rho}_l(\mu_q,|\mu|,\phi_r,\tilde{\phi})\mu_q J(\tau=0,-\mu_q,\phi_r\,|\,\tau_{t,s},\mu'') \tag{39}$$

So, we obtain the final expression for $\tilde{K}_l$ in Eq. (35):

$$\tilde{K}_l(\mu,\mu_i,\phi,\phi_j\,|\,\tau_{t,s})=\sum_{q=1}^p\sum_{r=1}^m w_q\beta_r\left[\tilde{\rho}_l(\mu_q,|\mu|,\phi_r,\phi-\phi_j)+\tilde{\rho}_l(\mu_q,|\mu|,\phi_r,\phi+\phi_j)\right]\mu_q J(\tau=0,-\mu_q,\phi_r\,|\,\tau_{t,s},\mu_i) \tag{40}$$

Pre-computed values of transmitted radiance $I(\tau_{t,s},\mu_i,\phi_j\,|\,\tau_{t,s},\mu_{0,s})$ are needed to evaluate the second term on the right-hand side. Eq. (35) requires values of the kernels $K_l(\mu,\mu_i,\phi\pm\phi_j\,|\,\tau_{t,s})$ only at the quadrature points of its second argument which comes into Eq. (39) only as direction of incidence in radiance *J*. Therefore, in order to perform iterative evaluations with Eq. (35), radiance *J* must be pre-computed for all SZAs $\arccos(\mu_i)$ and all possible combinations $\{\arccos(-\mu_i),\phi_j\}$ comprising directions of reflection. We see from Eq. (34) that radiance *J* also must be pre-computed at the level $\tau_{t,s}-\tau_s$ (difference between the total optical thickness and the optical depth of the observer, if sensor is at TOA level then we need transmitted radiance at $\tau_{t,s}$) $J(\tau_{t,s}-\tau_s,-\mu_s,\phi_j\,|\,\tau_{t,s},\mu_i)$ for all SZAs $\arccos(\mu_i)$ and all possible combinations $\{\arccos(-\mu_s),\phi_j\}$ comprising directions of transmission (bear in mind that $\mu_s<0$ defining direction of observation "s")

From Eq. (34) we see that surface reflected radiance at the surface level is needed at the following directions: for each observation (measurement) characterized with its own total optical thickness $\tau_{t,s}$ and SZA $\mu_{0,s}$ $(\mu_s < 0, \phi_s)$, $(-\mu_i, \phi_s \pm \phi_j)$, and, for the purpose of iterative process itself, $(-\mu_i, \phi_j)$. Eq. (35) gives these evaluations:

$$L_l^{(n)}(\tau_{t,s}, \mu_s < 0, \phi_s \mid \tau_{t,s}, \mu_{0,s}) = S_l(\mu_s < 0, \phi_s \mid \tau_{t,s}, \mu_{0,s}) + \sum_i^p \sum_j^m w_i \beta_j \tilde{K}_l(\mu_s, \mu_i, \phi_s, \phi_j \mid \tau_{t,s}) L^{(n-1)}(\tau_{t,s}, -\mu_i, \phi_j \mid \tau_{t,s}, \mu_{0,s}) \quad (41)$$

$$L_l^{(n)}(\tau_{t,s}, -\mu_i < 0, \phi_j \mid \tau_{t,s}, \mu_{0,s}) = S_l(-\mu_i < 0, \phi_j \mid \tau_{t,s}, \mu_{0,s}) + \sum_g^p \sum_h^m w_g \beta_h \tilde{K}_l(-\mu_i, \mu_g, \phi_j, \phi_h \mid \tau_{t,s}) L^{(n-1)}(\tau_{t,s}, -\mu_g, \phi_h \mid \tau_{t,s}, \mu_{0,s}) \quad (42)$$

$$L_l^{(n)}(\tau_{t,s}, -\mu_i < 0, \phi_s \pm \phi_j \mid \tau_{t,s}, \mu_{0,s}) = S_l(-\mu_i < 0, \phi_s \pm \phi_j \mid \tau_{t,s}, \mu_{0,s}) + \sum_g^p \sum_h^m w_g \beta_h \tilde{K}_l(-\mu_i, \mu_g, \phi_s \pm \phi_j, \phi_h \mid \tau_{t,s}) L^{(n-1)}(\tau_{t,s}, -\mu_g, \phi_h \mid \tau_{t,s}, \mu_{0,s}) \quad (43)$$

It is easy to see from Eq. (34) that the sums $S_l(-\mu_i < 0, \phi_s - \phi_j \mid \tau_{t,s}, \mu_{0,s}) + S_l(-\mu_i < 0, \phi_s + \phi_j \mid \tau_{t,s}, \mu_{0,s})$ and $\tilde{K}_l(-\mu_i, \mu_g, \phi_s - \phi_j, \phi_h \mid \tau_{t,s}) + \tilde{K}_l(-\mu_i, \mu_g, \phi_s + \phi_j, \phi_h \mid \tau_{t,s})$ are needed, not their separate values.

4. NUMERICAL TESTING OF THE ALGORITHM

Observed surface-reflected radiance *L* at the top-of-atmosphere (TOA) level was computed by solving the boundary value problem given by Eqs. (1), (2), and (3) with DISORT [18] using 158 streams. Radiances *I* and J were also computed with DISORT using the same computational scheme for all geometric conditions needed to run the retrievals and listed in the previous section. The values of *L* computed for randomly generated sun-to-sensor geometries of observation mimicking MODIS Terra conditions are used as simulations of experimental measurements. Fig. 1 shows distributions of Sun zenith, view zenith, and relative azimuth angles for an actual MODIS granule in the mid-latitude along with probability density functions of SZA and RAA used for random selections of geometric conditions. VZA was also randomly selected from [0°, 66°] range. Figure 2 presents 4 sets of 12 randomly selected geometric conditions.

Numerical tests were conducted with the following atmospheric conditions: the atmosphere is a uniform layer comprised with a) Rayleigh scattering and weak gas absorption, so that single scattering albedo (SSA) is 0.999 and optical thickness τ_R of 0.1 (this roughly corresponds to the wavelength of 550 nm) and b) transported mineral dust (MITR) and insoluble (INSO) aerosol models from OPAC [19] with optical thicknesses τ_A of 0.1, 0.5, and 1.0. Single scattering properties of aerosol were computed with code SPHER [20] at the wavelength of 550 nm.

Figure 3 shows TOA radiance *L* for two different aerosol type loads with the same surface conditions. It is clear that MITR aerosol model provides less noisy solution compare to INSO model. The noticeable difference between these two aerosol models is that MITR phase function contains only 138 terms in its Legendre polynomial expansion while INSO phase function contains 487 terms. The number of streams in the discrete ordinate calculations was chosen to avoid Delta-M truncation of the phase function (used in DISORT) for one of the aerosols. In the case of 158 streams scheme used in this study the truncation fraction is ~0.017 for INSO aerosol. Study [21] compared radiance *L* at the *surface level* directly computed with DISORT with numerical solution of Eq. (14) using radiance *I* and *J* also computed with DISORT. It was found that the DISORT solution had noticeable azimuthal noise of the order of few per cent, see Figures 1 – 3 there. The noisy pattern of *L* at the *surface level* reported in [21] is qualitatively similar to that of *L* at the TOA level in Figure 3. Though analysis of the origin of this noise is beyond the scope of this study, its presence in the solution makes it a valuable opportunity to check robustness of BRDF retrievals by the iterative process described above.

Surface-reflected radiance was computed for two BRDF models. First, bare soil model by Nilson and Kuusk [22], see equations (11) and (11') there:

$$\rho(\theta_s,\theta_v,\phi) = a\left(b_0 + b_1\theta_s\theta_v\cos\phi + b_2\left(\theta_s^2+\theta_v^2\right) + b_3\theta_s^2\theta_v^2\right)$$
$$a = \lim_{\theta_s\to\pi/2} a(\theta_s) = 0.2; \quad b_0 = 0.31489; \quad b_1 = 0.14129; \quad b_2 = -0.082511; \quad b_3 = 0.14779 \tag{44}$$

The main purpose of the use of this BRDF is to check whether the algorithm can resolve more than 3 kernels.

The second model is MODIS BRDF, see [15] equations (37) – (44):

$$\rho(\theta_s,\theta_v,\phi) = \frac{1}{\pi}\left(f_{iso} + f_{vol}K_{vol}(\theta_s,\theta_v,\phi) + f_{geo}K_{geo}(\theta_s,\theta_v,\phi)\right) \tag{45}$$

where factor $1/\pi$ comes in due to the difference in definitions, so that we will denote $\alpha_1 = f_{iso}/\pi$, $\alpha_2 = f_{vol}/\pi$, $\alpha_3 = f_{geo}/\pi$. Particular values of the weights are picked up from actual MODIS BRDF products. The values are chosen to shoe how zero and small weights are resolved and how the number of observations and optical thickness of the atmosphere affect the retrievals.

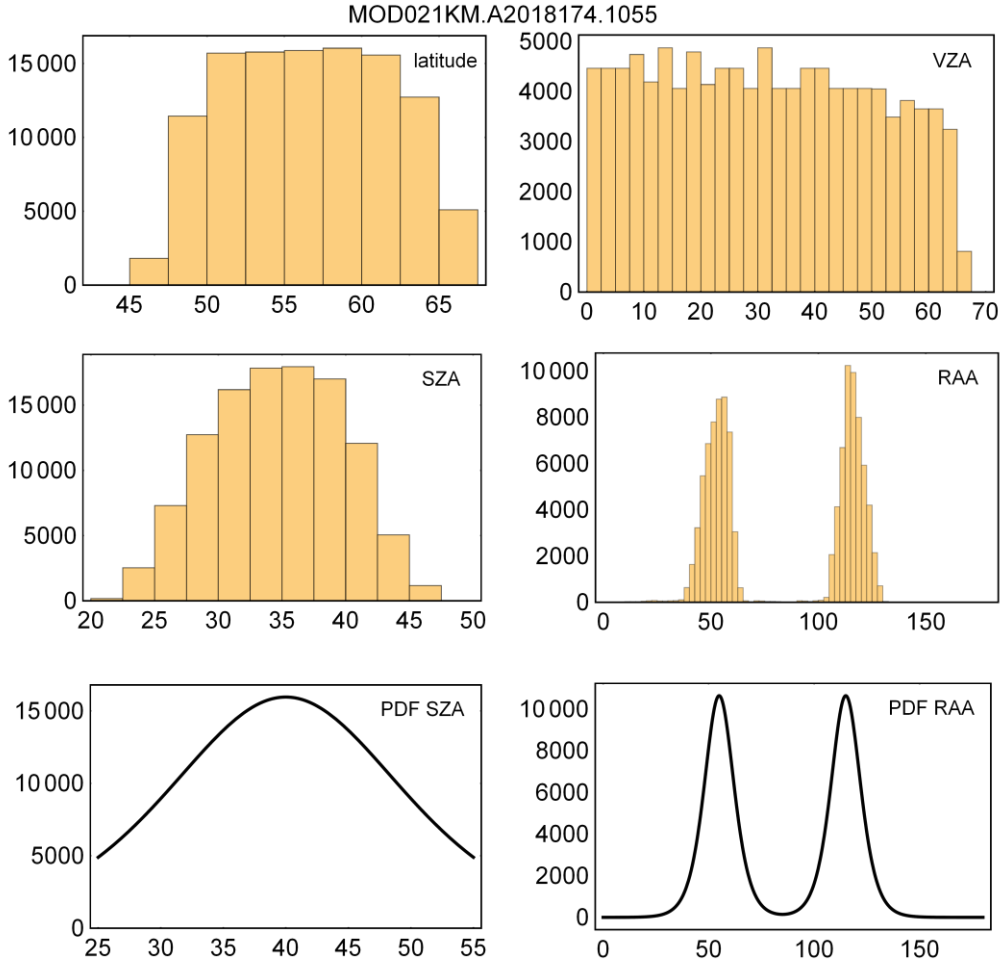

Figure 1. A Distributions on latitude (top left), view zenith angle (top right), sun zenith angle (middle left), and relative azimuth angle (middle right) for a MODIS image. Probability density functions of the sun zenith and relative azimuth angles (bottom left and right, respectively) used to model geometries of observations.

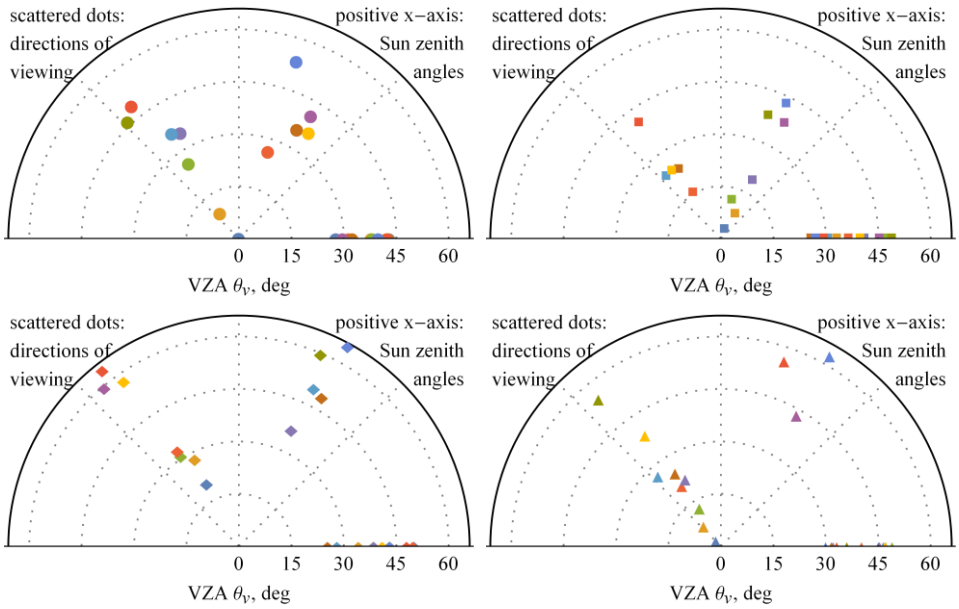

Figure 2. Four randomly selected sets of 12 geometries of observations.

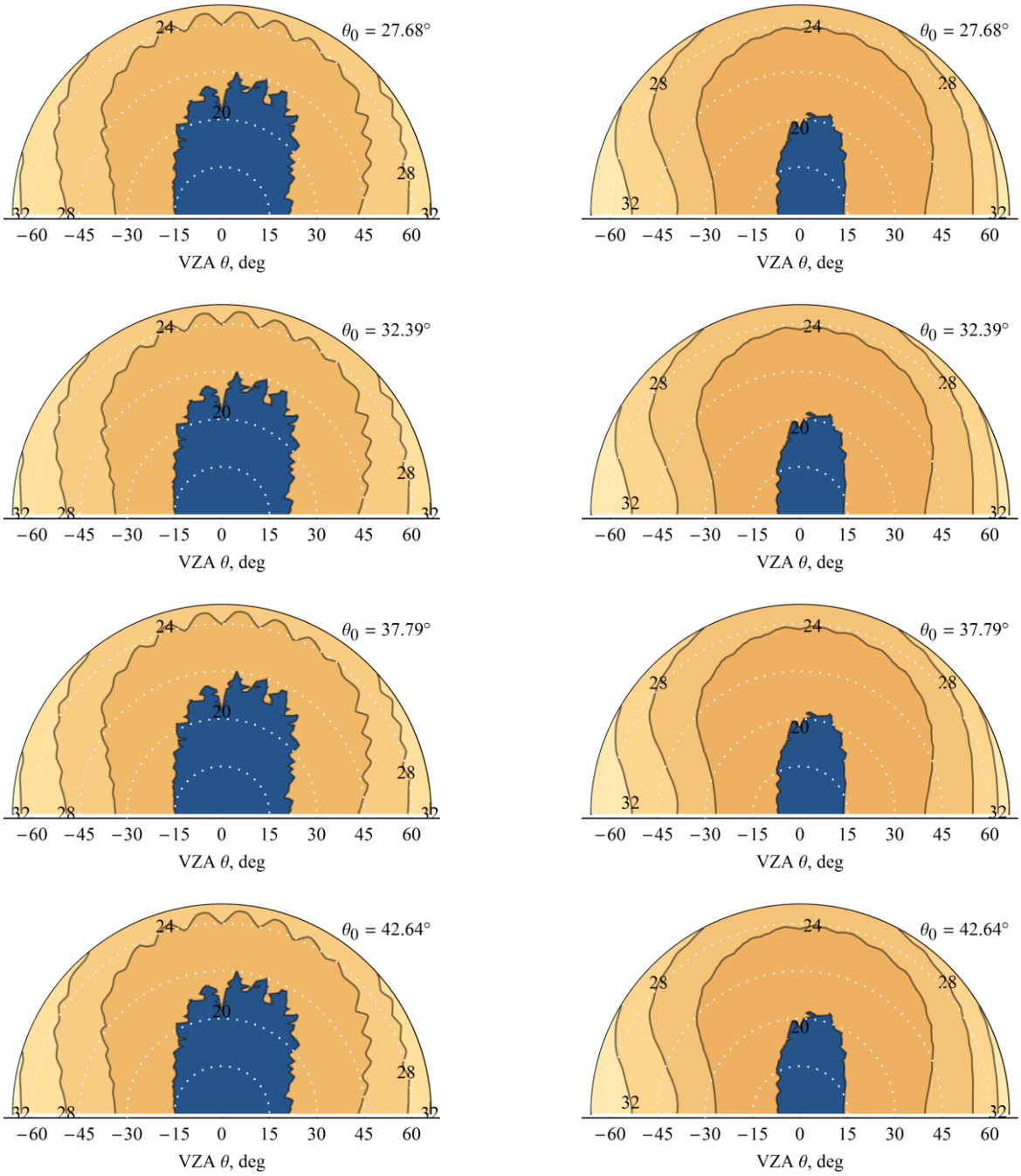

Figure 3. Reflected radiance at the top of atmosphere level for MODIS BRDF model, Eq. (45), with parameters f_{iso} = 0.067, f_{vol} = 0.031, f_{geo} = 0.014 (see Fig. 6 for the source of data) and INSO aerosol of $\tau_A = 0.1$ (left panels) and MITR aerosol of $\tau_A = 0.1$ (right panels) under the same illumination conditions.

Figure 4 shows retrieval of the kernel weights for Nilson – Kuusk BRDF, Eq. (44), for optical two thicknesses of the atmosphere and 4 different randomly selected sets of 12 observations. It is clear that increase of the optical thickness causes greater spread of the retrieved kernel weights. Weights of the first two kernels are retrieved with accuracy better than 5% for $\tau_t = \tau_R + \tau_A = 0.2$ and better than ~6% for $\tau_t = 0.6$. However, 3rd and 4th weights are retrieved with accuracy better than 10% for $\tau_t = 0.2$ and around 20% for $\tau_t = 0.6$. It is interesting to note that for both optical thicknesses the pattern is that if α_3 is overestimated than corresponding α_4 is underestimated and vise versa.

Figure 5 shows retrievals of the kernel weights for MODIS BRDF, Eq. (45), with TOA modeling performed for f_{iso} = 0.080, f_{vol} = 0.129, f_{geo} = 0.000. These and all subsequent kernel values are taken from MODIS BRDF product [23]. Both non-zero weights α_1, α_2 are retrieved with accuracy around 5% for both INSO and MITR aerosols though aerosol optical thickness of the latter is 1.0 while it is 0.1 for the former. It is hardly possible to observe optically thick load of insoluble aerosol while mineral transport is the primary aerosol constituent in the dust storms. Before discussing accuracy of retrievals of weight α_3 which is zero in this case, it is important to mention that MODIS BRDF product provides weights with 3 decimal places so that f_{iso}, f_{vol}, and f_{geo} can take values 0.000, 0.001, 0.002, and so on. Values on the vertical axis of the very bottom row of Fig. 4 are given with this precision of the original product. We see that 3 out of 4 retrievals provide $|f_{geo}| < 0.001$ while one gives $f_{geo} \sim 0.005$ for INSO aerosol of $\tau_A = 0.1$ (left panel) while $|f_{geo}|$ slightly exceeds 0.001 for 1 retrieval for MITR aerosol of $\tau_A = 1.0$. Thus, zero weight of one kernel was successfully retrieved.

Left panels in Figure 6 shows retrievals in the situation with one weight being small: $f_{vol} = 0.001$. Retrieved values of that kernel weight range from -0.006 to 0.005. MODIS BRDF model does not allow negative kernel values. So, if iterative process returns a negative value it has to be set zero with repeating the iterative process. This has not been done in this study. At the same time weight α_1 was retrieved with accuracy better than 5% while α_3 is slightly beyond that margin for one particular set of geometric conditions. Right panels in Figure 6 present a general case with all weights being not small. All for retrievals of α_1, 3 of α_2, and 2 of α_3 are within 5% accuracy, while the rest are within 10%.

5. CONCLUSION

An algorithm for retrievals of BRDF from the surface-reflected radiance measured at any level of the atmosphere is presented. The algorithm is based on the expression of the radiance in the atmosphere underlain by anisotropic reflecting surface through the solutions of the RT problems for un-bound atmosphere and surface BRDF. The presented algorithm requires an assumption on the atmospheric condition. It is based on kernel-based BRDF; therefore, it also requires an assumption on the functional form of the kernels comprising BRDF. The algorithm returns the weights of the kernels. The choice of the kernels depends on the physical properties of the surface.

The previous analysis of the different terms of Eq. (14) governing reflected radiance at the surface level suggested that the contribution of the source term of the equation is crucial. Therefore, fast convergence of the iterative process could be expected since the source term of Eq. (14) defines the initial approximation of the radiance above the surface. In all considered cases kernel weights are visually indistinguishable after 1st iteration though their values may change in 4th significant figure. There was no case the iterative process has not converge though there are many cases when kernel weights retrieved with error of more than 5%, sometimes worse than 20%. These errors can be mostly attributed to the noisy simulated input radiances used in the presented retrievals: cases with INSO aerosol are always less accurate than those with MITR since the simulated radiances are less noisy in the latter case.

Accuracy of the algorithm depends on the number of experimental measurements used for retrievals, optical thickness of the atmosphere, and the quality of the measurements of the surface-reflected radiance. The last two factors may not be independent in the context of this study since the surface-reflected radiance was simulated with DISORT. Retrievals were performed on the sets of 12, 24, and 60 randomly selected sun-to-sensor geometries. Generally, the more observations are used the more accurate retrievals are. Also, increasing aerosol optical thickness decreases accuracy of the retrievals. However, accurate retrievals were performed for aerosol optical thicknesses up to 1.0.

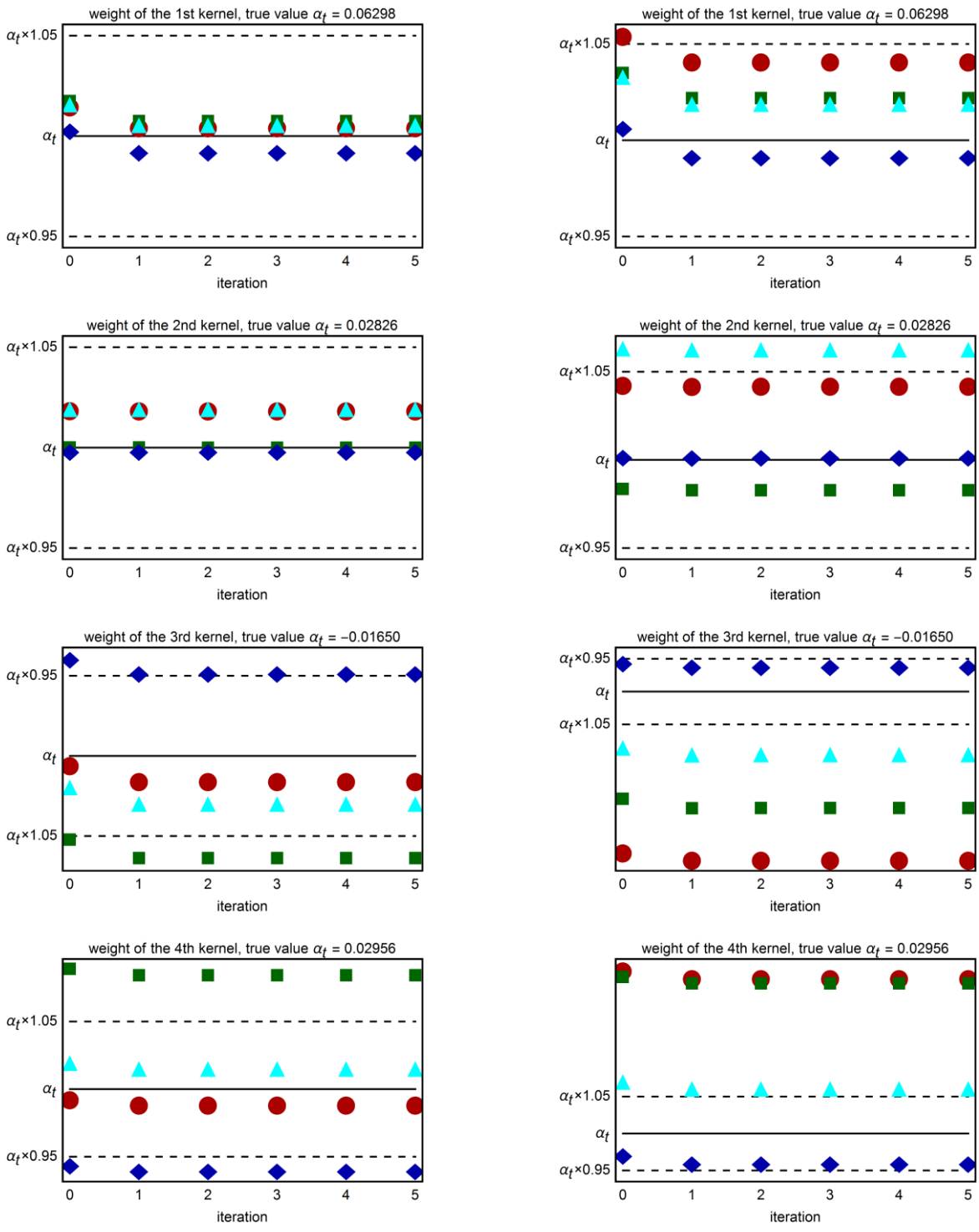

Figure 4. Iterations of the kernel weights for Nilson – Kuusk BRDF, Eq. (44). Four sets of 12 randomly selected geometric conditions. Left panels – optical thickness of the atmosphere $\tau_t = \tau_R + \tau_A = 0.2$, right panels - $\tau_t = 0.6$. Aerosol type – MITR.

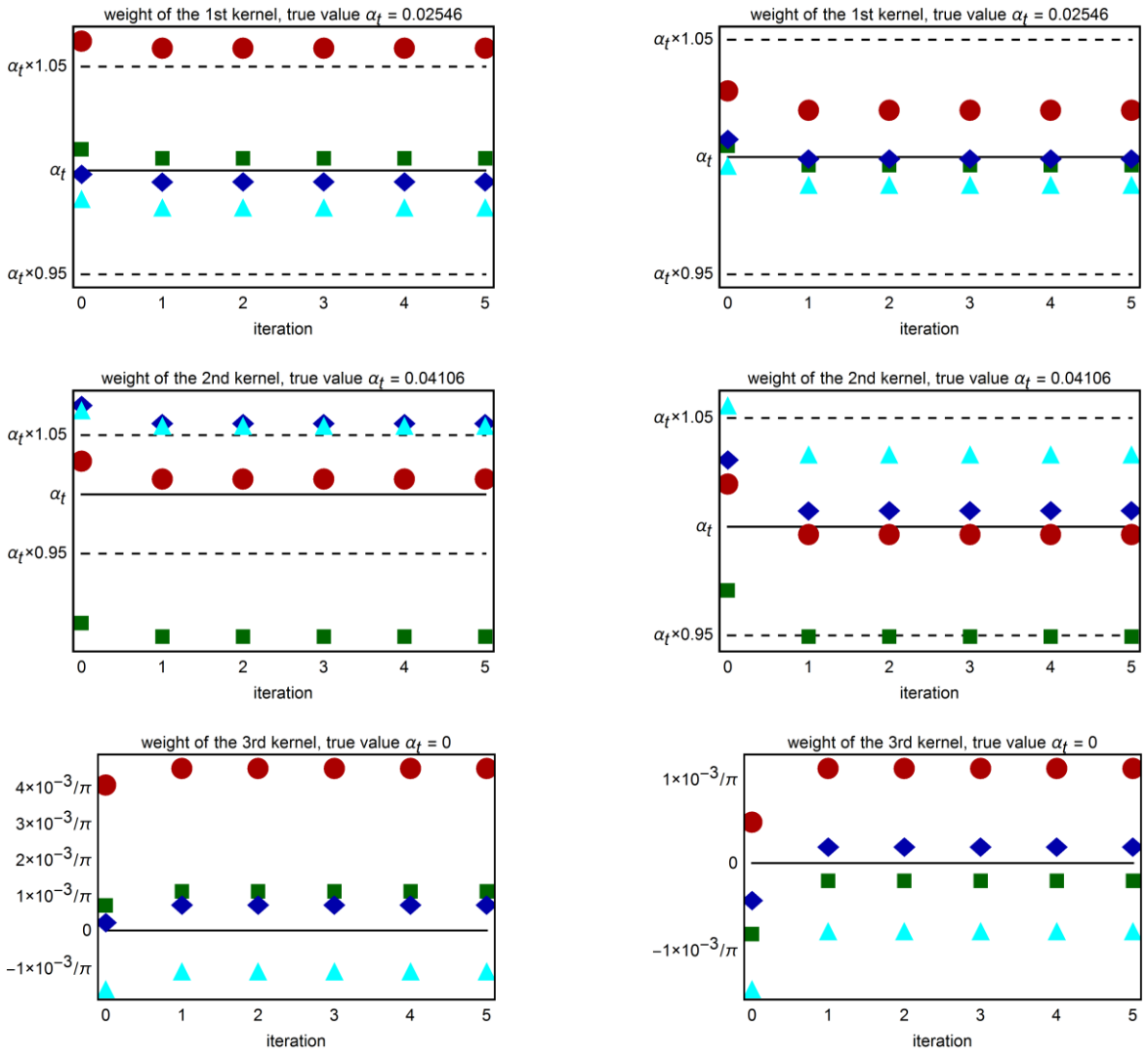

Figure 5. The same as Fig. 3 but for MODIS BRDF, Eq. (45), for f_{iso} = 0.080, f_{vol} = 0.129, f_{geo} = 0.000. BRDF parameters are taken from MCD43C1.A2018207.006.2018221014951.hdf, for band 4 (550 nm), pixel (1441, 735) (numbered from 0); center latitude = 53.225N, longitude = 107.925W (Medstead No. 497, SK, Canada). Four sets of 24 randomly selected geometric conditions. Left panels – optical thickness of the atmosphere $\tau_t = 0.2$ with INSO aerosol; right panels - $\tau_t = 1.1$, MITR aerosol.

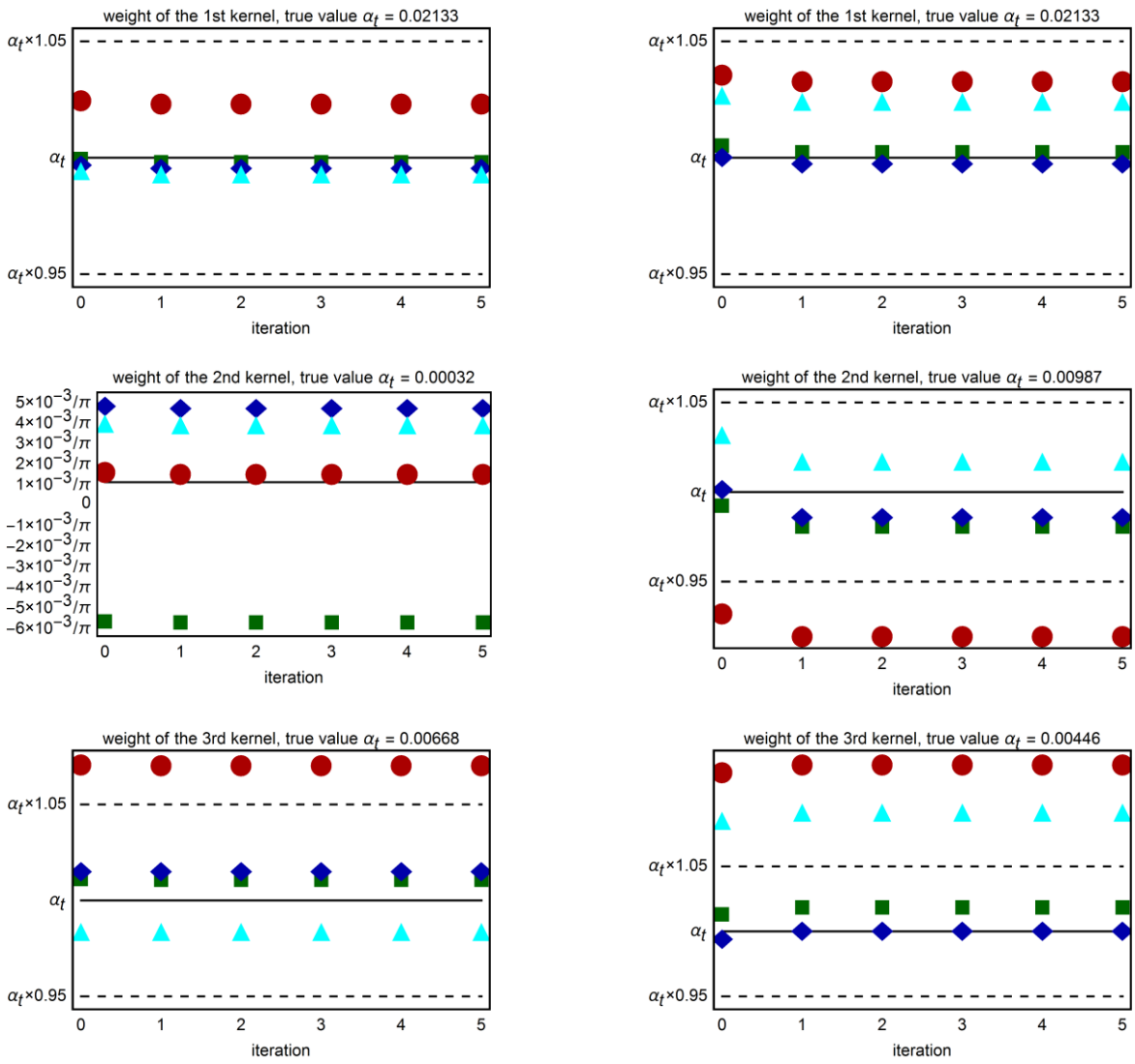

Figure 6. The same as Fig. 4 but for two different surface and atmospheric conditions. Left panels: BRDF parameters f_{iso} = 0.067, f_{vol} = 0.001, f_{geo} = 0.021 are taken from MCD43C1.A2018207.006.2018221014951.hdf for band 4 (550 nm), pixel (1383, 577), (numbered from 0), center latitude = 61.125N, longitude = 110.825W (Canada, NT), and INSO aerosol with total optical thickness of the atmosphere $\tau_t = 0.2$; four sets of 24 randomly selected geometric conditions. Right panels: BRDF parameters f_{iso} = 0.067, f_{vol} = 0.031, f_{geo} = 0.014 are taken from MCD43C1.A2018207.006.2018221014951.hdf for band 4 (550 nm), pixel (1680, 742) (numbered from 0), center latitude = 52.875N, longitude = 95.975W (Poplar/Nanowin Rivers Park Reserve, Manitoba, Canada), and MITR aerosol with total optical thickness $\tau_t = 0.6$.

References

[1] Sayer, A.M., Thomas, G.E., Grainger, R.G., Carboni, E., Poulsen, C., and Siddans, R., "Use of MODIS-derived surface reflectance data in the ORAC-AATSR aerosol retrieval algorithm: Impact of differences between sensor spectral response functions." Remote Sensing of Environment, 116, 177 - 188 (2012).

[2] Platnick, S., King, M.D., Ackerman, S.A., Menzel, W.P., Baum, B.A., Riedi, J.C., and Frey, R.A., "The MODIS cloud products: algorithms and examples from Terra," IEEE TGRS, 41, 459 – 473 (2003).

[3] Wang Z., Schaaf, C.B., Sun, Q., Shuai, Y., and Román, M.O., "Capturing rapid land surface dynamics with Collection V006 MODIS BRDF/NBAR/Albedo (MCD43) products," Remote Sensing of Environment, 207, 50 – 64 (2018).

[4] Strahler, A.H., Muller, J.-P., and co-authors, "MODIS BRDF/Albedo Product: Algorithm Theoretical Basis Document", available at https://modis-land.gsfc.nasa.gov/pdf/atbd_mod09.pdf

[5] Wanner, W., Strahler, A.H., Hu, B., Lewis, P., Muller, J.-P., Li, X., Schaaf, C.L.B., and Barnsley M.J., "Global retrieval of bidirectional reflectance and albedo over land from EOS MODIS and MISR data: Theory and algorithm," J. Geophys. Res. 102(D14), 17143 – 17161 (1997).

[6] Vermote, E.F., Saleous, N.E., Justice, C.O., Kaufman, Y.J., Privette, J.L., Remer, L., Roger, J.C., and Tanre, D., "Atmospheric correction of visible to middle-infrared EOS-MODIS data over land surfaces: Background, operational algorithm and validation," J. Geophys. Res. 102(D14), 17131 – 17141 (1997).

[7] Lyapustin, A., Martonchik, J.; Wang, Y.; Laszlo, I.; Korkin, S. Multi-Angle Implementation of Atmospheric Correction (MAIAC): Part 1. Radiative Transfer Basis and Look-Up Tables. J. Geophys. Res. 116, D03210 (2011).

[8] Lyapustin, A., Wang, Y., Laszlo, I., Kahn, R., Korkin, S., Remer, L., Levy, R., and Reid, J.S., "Multiangle implementation of atmospheric correction (MAIAC): 2. Aerosol algorithm," J. Geophys. Res., 116, D03211 (2011).

[9] Lyapustin A.I., Wang, Y., Laszlo, I., Hilker, T., Hall, F.G., Sellers, P.J., Tucker, C.J., Korkin, S.V., "Multi-angle implementation of atmospheric correction for MODIS (MAIAC): 3. Atmospheric correction," Remote Sensing of Environment, 127, 385-393 (2012).

[10] Lyapustin, A.I.; Knyazikhin, Y., "Green's function method for the radiative transfer problem. I. Homogeneous non-Lambertian surface," Appl. Opt., 40, 3495–3501 (2001).

[11] Radkevich, A., "A new look at decoupling of atmospheric radiative transfer and anisotropic surface reflection," JQSRT, 127, 140–148 (2013).

[12] Radkevich, A., "A Method of Retrieving BRDF from Surface-Reflected Radiance Using Decoupling of Atmospheric Radiative Transfer and Surface Reflection," Remote Sensing, 10, 591 (2018).

[13] Roujean, J.-L.; Leroy, M.; Deschamps, P.Y., "A bidirectional reflectance model of the Earth's surface for the correction of remote sensing data," J. Geophys. Res., 97, 20455–20468 (1992).

[14] Lewis, P., "The utility of kernel-driven BRDF models in global BRDF and albedo studies," Proc. of the Geoscience and Remote Sensing Symposium, (1995), doi:10.1109/IGARSS.1995.521179.

[15] Lucht, W., Schaaf, C.B., Strahler, A.H., "An algorithm for the retrieval of albedo from space using semiempirical BRDF models," IEEE Trans. Geosci. Remote Sens. 2000, 38, 977–998 (2000).

[16] Liu, S., Liu, Q., Liu, Q., Wen, J., Li, X., "The Angular and Spectral Kernel Model for BRDF and Albedo Retrieval," IEEE J. Sel. Top. Appl. Earth Obs. Remote Sens., 3, 242–256 (2010).

[17] Roujean, J.-L., "Inversion of Lumped Parameters Using BRDF Kernels," Comprehensive Remote Sensing, 3, 23–34 (2018).

[18] Stamnes K, Tsay S-C, Wiscombe W, Laszlo I. DISORT, a General-Purpose Fortran Program for Discrete-Ordinate-Method Radiative Transfer in Scattering and Emitting Layered Media: Documentation of Methodology. DISORT Report v1.1, March 2000, available at http://lllab.phy.stevens.edu/disort/docs/DISORTReport1.1.pdf

[19] Hess, M., Koepke, P., and Schult, I. Optical Properties of Aerosols and Clouds: The Software Package OPAC, BAMS, 1998, 79, 831-844, doi.org/10.1175/1520-0477(1998)079<0831:OPOAAC>2.0.CO;2.

[20] Mishchenko, M.I., Travis, L.D., and Lacis, A.A. Scattering, Absorption, and Emission of Light by Small Particles. Cambridge University Press, Cambridge, UK, 2002; 448 pp, ISBN: 9780521782524. Code available at https://www.giss.nasa.gov/staff/mmishchenko/ftpcode/spher.f.

[21] Radkevich A. Iterative discrete ordinates solution of the equation for the surface-reflected radiance. JQSRT, 2017, v. 202, p. 114 – 125.

[22] Nilson, T. and Kuusk, A., "A reflectance model for the homogeneous plant canopy and its inversion," Remote Sens. Environ., 1989, 27, 157-167, https://doi.org/10.1016/0034-4257(89)90015-1.

[23] Crystal Schaaf - University of Massachusetts Boston, Zhuosen Wang - NASA GSFC and MODAPS SIPS - NASA. (2015). MCD43C1 MODIS/Terra+Aqua BRDF/Albedo Model Parameters Daily L3 0.05Deg CMG. NASA LP DAAC. http://doi.org/10.5067/MODIS/MCD43C1.006